ACS Photonics

Open Access

pubs.acs.org/journal/apchd5

Letter

Intracavity Epsilon-Near-Zero Dual-Range Frequency Switch

Jiaye Wu,* Gang Wang, Marco Clementi, Ji Zhou, Chenxingyu Huang, Xuanyi Liu, H. Y. Fu, Qian Li, and Camille-Sophie Brès*

Cite This: ACS Photonics 2025, 12, 1276−1283

Read Online

ACCESS | Metrics & More | Article Recommendations | Supporting Information

ABSTRACT: Epsilon-near-zero (ENZ) nanophotonic devices with zero permittivity are known to exhibit adiabatic frequency translation via temporal refraction under extracavity excitation by intense light sources, which are however hard to integrate on-chip owing to a high demand for energy density. As this class of complementary-metaloxide-semiconductor-compatible materials is progressing toward on-chip photonic integration, a more versatile solution with less intensity requirements needs to be further explored. Here, for the first time, by leveraging the abundant frequency mode resources inside a resonant cavity, we experimentally demonstrate the realization of input-dependent dual-range frequency switching via a single intracavity ENZ element. By utilizing the linear and nonlinear effects induced by ENZ, the system can perform a small 279.73 GHz as well as a 13-octave-span larger (3.63-THz) mode-locked frequency shift at 196 and 192 THz, respectively, under a pulse energy 2 orders of magnitude lower than extracavity schemes with a conversion efficiency (in %frequency shift per unit energy density per unit material thickness) also 2 orders of magnitude higher. Additionally, we report for the first time the real-time observation of the intracavity ENZ frequency switching operation, proving that the mechanism differs from pure ENZ time refraction. We further discuss that by encoding the states of two intracavity components, the optical system can program eight types of different 1- and 2-operand logic functions, including four complex noncommutative ones. This work extends the understanding of ENZ photonics beyond extracavity scenarios. The proposed solution could be extended to photonic integration with a potential for novel optical logic gates and photonic computing designs as an efficient and simplified alternative to microelectronic counterparts.

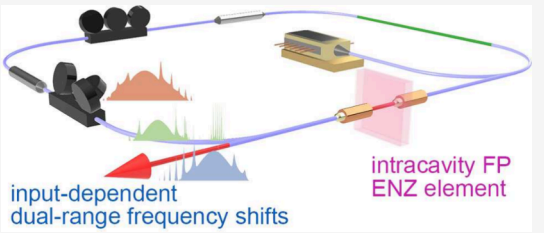

KEYWORDS: *epsilon-near-zero, active cavity, frequency switching, indium tin oxide, conversion efficiencies*

INTRODUCTION

Featuring a zero crossover of its real permittivity, epsilon-near-zero (ENZ) photonic materials exhibit exotic linear and nonlinear optical behaviors that are otherwise nonachievable by conventional optical materials.[1−3] ENZ platforms such as radio frequency (RF) metamaterials,[4,5] nanophotonic metamaterials,[6,7] and the complementary metal-oxide-semiconductor (CMOS)-compatible transparent conducting oxide (TCO)[8−10] family enable the tunneling of unchanged phase,[11] new frequency generation,[9,12−18] giant enhancements of electric fields,[19] Kerr nonlinearity,[8] thermo-optic effect, and thermo-optic nonlinearity.[10] These rich phenomena also allow the photonic emulation of physical systems in distant disciplines of research,[4,5,15,20−22] inspiring novel and deeper insights in both photonics and emulated fields.

Due to the intrinsic excitation threshold, the relatively high loss, limited number, and duration of interactions, most of the reported extracavity nonlinear frequency conversions through ENZ temporal refractions require strong laser sources such as solid-state Ti:sapphire lasers with an intensity up to several hundreds of gigawatts per squared centimeter.[15,23−25] As the CMOS-compatible ENZ TCOs evolve toward photonic integrated chips (PICs),[26,27] one of the bottlenecks is the demand for an intense, integratable, and compact light source. One possible solution to this obstacle is to employ an ENZ material in an intracavity fashion instead of the conventional extracavity scheme to benefit from cumulative interactions. Unlike the extracavity cases, where the system is passive, the intracavity condition is non-Hermitian and provides much richer frequency resources to select from and convert to. Still, research on intracavity ENZ is rare.

For the studies on intracavity ENZ effects, the state-of-the-art includes Q-switching by ENZ saturable absorption,[28−30] mode-locking (ML) by transient bleach,[31] hybrid ML behaviors,[21] and vortex beam generation with orbital angular momentum.[6] Among them, the ones mentioning intracavity frequency shifts are even more scarce.[21,30] They lack frequency-shift versatility; i.e., they can perform a short-range frequency shift of ≈200 GHz[30] or a long-range frequency shift of ≈2 THz[21] which cannot coexist with each other. The fact

Received: July 18, 2024
Revised: November 28, 2024
Accepted: December 2, 2024
Published: December 5, 2024

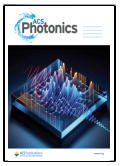

https://doi.org/10.1021/acsphotonics.4c01322
ACS Photonics 2025, 12, 1276−1283

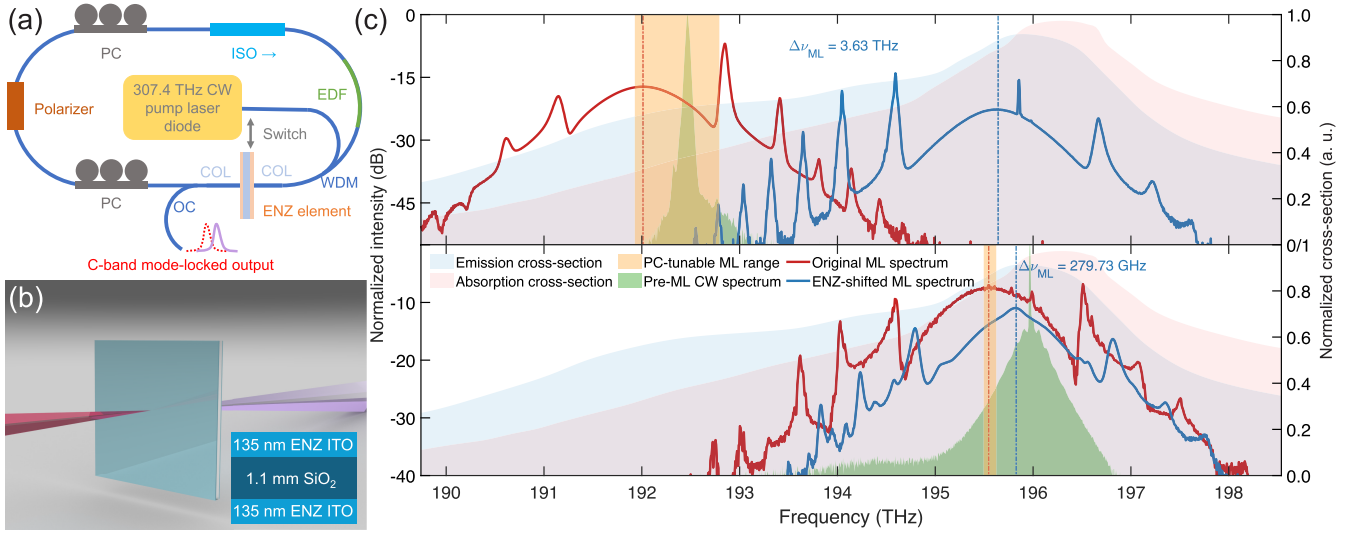

Figure 1. Intracavity epsilon-near-zero (ENZ) mode-lock (ML) frequency switch operations. (a) Setup of the intracavity ENZ laser system. (b) The schematic diagram of the ENZ Fabry-Pérot indium tin oxide nanostructure. The inset shows the structure of the sample's cross-section (not to scale). (c) Intracavity ML frequency shifts at 192 and 196 THz beyond the intrinsic polarization-tunable range. COL: collimator; CW: continuous wave; EDF: erbium-doped fiber; ISO: optical isolator; OC: output coupler; PC: polarization controller; WDM: wavelength division multiplexer.

that they operate either in a continuous wave (CW) mode or in one single pulsed (ML/Q-switched) mode only allows them to function as an operation-mode switch (pulse ↔ CW) rather than a practical intracavity frequency selection. Besides, it remains unclear: (i) experimentally whether the ENZ-induced intracavity frequency shift is an adiabatic process as in the extracavity cases; (ii) quantitatively the efficiency advantages of an intracavity design over the conventional extracavity ones; and (iii) qualitatively the possible practical implementation and application such a photonic system can achieve.

Here, for the first time, we experimentally demonstrate the realization of dual-range frequency switching via an active optical system with a single intracavity ENZ Fabry-Pérot (FP) nanostructure. The intracavity ENZ FP element acts as an ML frequency switch by altering the mode-competition selectivity. Depending on the initial ML frequencies, it can induce either a 279.73-GHz or a 13-octave-span larger (3.63-THz) frequency shift while maintaining ML, far beyond the cavity's intrinsic continuously tunable range. To prove the benefits of using an intracavity design, we characterize the frequency conversion efficiencies in terms of the required pulse energy and ENZ TCO thickness. The pulse-energy efficiencies for the short-range shift are on par with the extracavity reports, while the long-range shift is leading in both metrics. Additionally, we employ the time-stretched discrete Fourier transform (TS-DFT) technique to study the real-time dynamics of the ENZ intracavity frequency switching operations, which are found to be based on mode reselection rather than adiabatic temporal refraction. It is further discussed that by encoding the polarization state and the ENZ-element state as either 0 or 1, the optical system can perform two 1-operand logic (TRUE and FALSE), two commutative 2-operand logic (AND and OR), as well as four complex noncommutative 2-operand logic (converse nonimplication, converse implication, material implication, and material nonimplication) all enabled by a single ENZ nanostructure. The idea and mechanism behind the proposed intracavity ENZ system is compatible with state-of-the-art photonic integration and nanophotonic platforms,[32] and we believe that the results of this work extend the understanding and the applications of ENZ photonics beyond the extracavity scenarios, beneficial to the development of integrated ENZ optical computing systems-on-chip.

RESULTS

Intracavity Dual-Range Frequency Switch Operations. For maximal generality, we construct the simplest form of a nonlinear polarization rotation (NPR) ML cavity with a 0.6 m erbium-doped fiber (EDF) pumped at 975.3 nm (307.4 THz), polarization controllers (PCs), an isolator, and a polarizer as depicted in Figure 1a. The free spectral range (FSR) of the cavity-generated ML frequency combs is 16 MHz. The key element of the cavity is an ENZ indium tin oxide (ITO) FP nanostructure inserted in between two collimators. The FP cavity medium is silica glass with a thickness of 1.1 mm and a theoretical FSR of 94.6 GHz, far higher than the FSR of the ML cavity, in order not to disturb the ML process (see Supporting Information S2.3 and S3.1), while enhancing light-matter interactions at the nanometer scale compared to a single layer. The ITO layer on both sides of the silica has a thickness of 135 nm, as illustrated in Figure 1b. The two ITO layers are fabricated with slightly different ENZ frequencies of 156.85 and 162.02 THz (see Supporting Information S1.1), providing a flat dispersion at the C-band while imprinting an FP-induced selectivity in the C-band which favors the dual-range frequency switching within the EDF gain spectrum (Supporting Information S1.5). In our supplementary experiments (Supporting Information S2.2), the 2-μm-band ENZ ITO monolayer which only lacks this feature cannot achieve mode-locking at C-band, while the C-band ENZ ITO monolayer can only perform single-range frequency switching, which are consistent with previous observations.[21]

Figure 1c shows various spectra of the intracavity ENZ ML frequency switch operations. The blue and red shades denote the emission and absorption cross sections of the EDF, with data extracted from the manufacturer test report. There exist two stable ML frequency ranges in the NPR cavity, intrinsic to the properties of EDF, namely, around 192 THz where the

https://doi.org/10.1021/acsphotonics.4c01322
ACS Photonics 2025, 12, 1276−1283

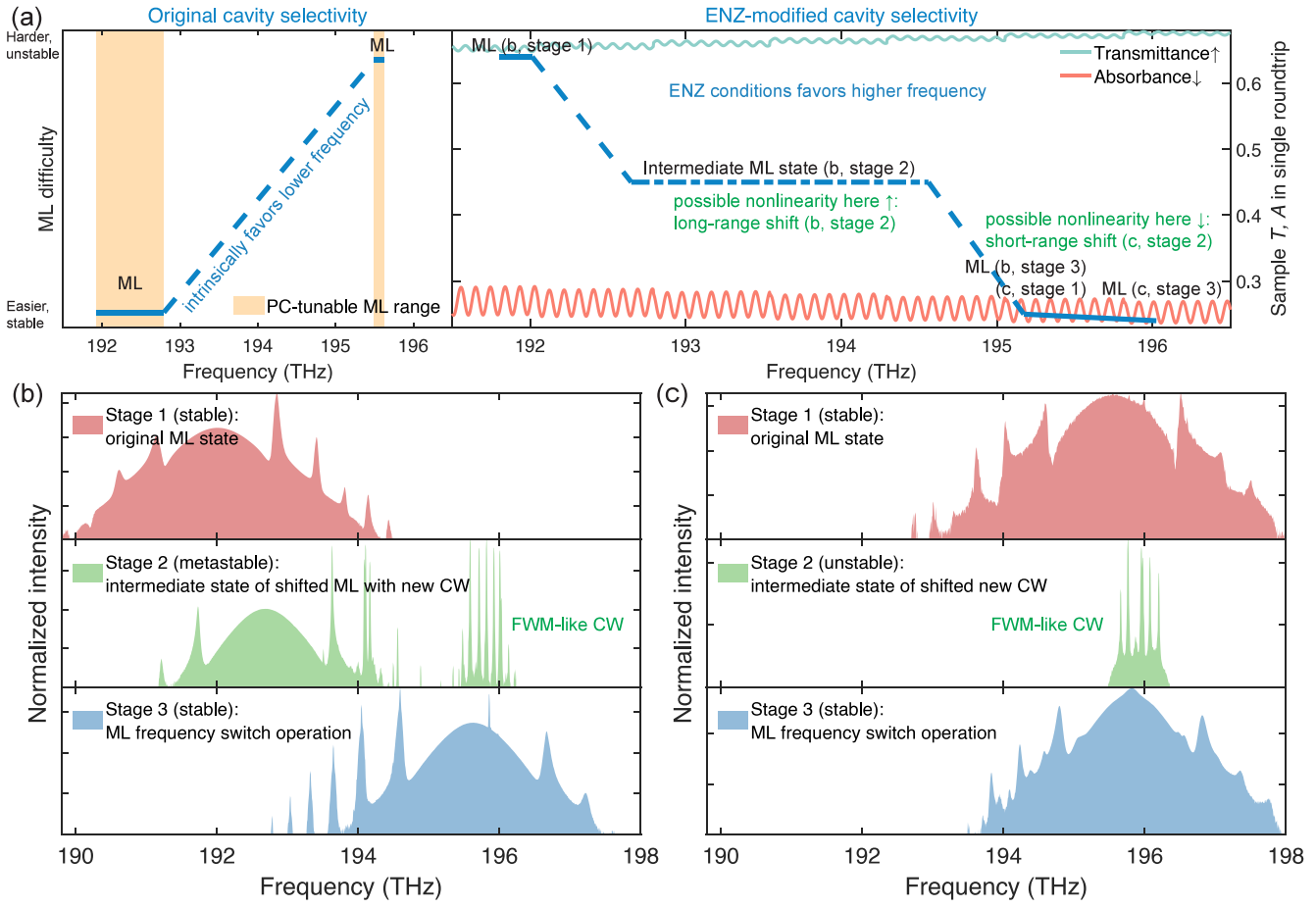

Figure 2. Mechanisms of intracavity frequency switch operations. (a) Schematic diagram of the stability and difficulty of mode-locking (ML) in different cases, illustrated in a style analogous to an energy-level system for intuitive understanding. A detailed analysis of possible contributing factors is presented in Supporting Information S1.5. Different stages of ML establishment in epsilon-near-zero-element-induced frequency switch operations (b) are for long-range shift and (c) for short-range shift.

difference between the emission and absorption cross-sections is the largest and 196 THz where the emission cross-section peaks while suffering also the highest absorption. The green spikes in both panels of Figure 1c represent the spectra of the CW output before the ML state is established. The yellow shades (relatively wide at 192 THz and barely visible at 196 THz) are defined as the "PC-tunable ML range" where the center frequency of the cavity can be continuously moved by rotating the PCs while maintaining the ML state, without the presence of the ENZ element. While without the ENZ element, the transitions between 192 THz and 196 THz ML states can also be achieved by tuning the PCs; once outside the defined PC-tunable ML range, the cavity operates in CW mode and a laborious search for a correct polarization state is needed to re-establish ML at the new frequency. Therefore, the transition process is neither seamless nor continuous.

Depending on which ML stable region the cavity is currently operating in and without any further controls on PCs, when the intracavity ENZ component is present, an intracavity ENZ ML frequency switch operation occurs. If the cavity has an initial ML state at 192 THz, the ENZ nanostructure shifts the center frequency 3.63-THz away from the original ML frequency instantaneously to reach the regime of 196 THz, far outside the PC-tunable ML range, referred to as the long-range shift. Alternatively, if the cavity is initially 196 THz, the ENZ nanostructure shifts the center frequency 279.73 GHz instantaneously (referred to as a short-range shift), also outside the PC-tunable ML range. The long-range shift is 13-octave-span larger than the short-range shift. This is nonachievable by conventional optical materials such as the substrate silica glass and can only be partially achieved (either a long-range[21] or a short-range frequency shift,[30] but not coexistent) by single-layered ENZ ITO (see Supporting Information S2.2).

The presence of the designed ENZ nanostructure alters the mode-competition selectivity of the NPR cavity, resulting in the observed switching actions. For intuitive understanding, we plot a schematic diagram of the ML state transitions before and after the ENZ element insertion in Figure 2a. The schematic is analogous to an energy-level system, whereas the lower the "energy", the easier and more stable the corresponding ML state can be achieved. In the original cavity without the ENZ element, ML is only possible within the PC-tunable range, while due to the high absorption of the EDF at 196 THz, the ML state is less stable and less tunable. This original mode-selectivity is intrinsic to the cavity, especially determined by the EDF gain spectrum. In the presence of the ENZ element, due to the higher loss in the ENZ ITO at lower frequencies shown in the right panel of Figure 2a, the ENZ loss counteracts the effect of EDF absorption, resulting in a modified ML tendency. As the overall loss increases, the ML pump threshold is relatively higher (see Supporting Information S3.1). Additionally, the transmittance spectrum favors a higher

https://doi.org/10.1021/acsphotonics.4c01322
ACS Photonics 2025, 12, 1276−1283

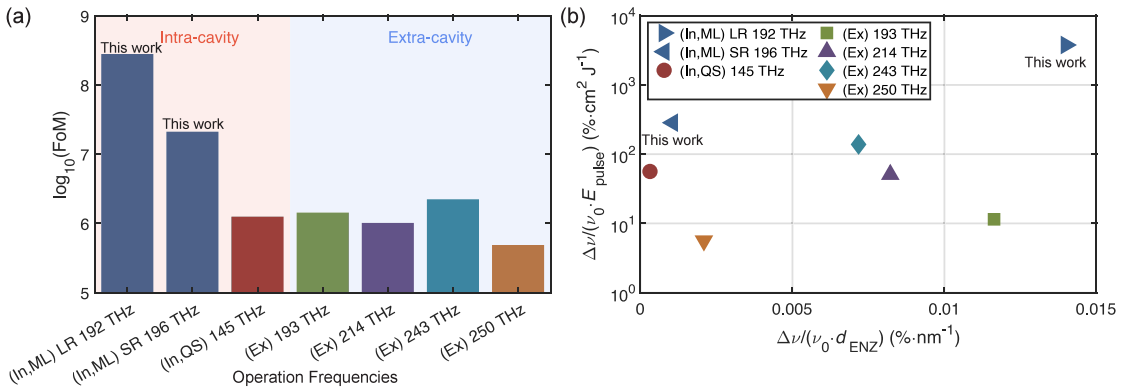

Figure 3. Efficient intracavity frequency switching. (a) Figure-of-merit comparison between intracavity and extracavity frequency shifting. The values in THz are their respective operation frequencies. (b) The energy (vertical axis) and thickness (horizontal axis) efficiencies of the intracavity and extracavity frequency shifting approaches. "In" denotes intracavity, and "Ex" represents extracavity. ML: mode-locked; QS: Q-switched. LR: long-range; SR: short-range. FoMs and efficiency data calculated: (In,ML) values from this work; (In,QS) 145 THz from ref 30; (Ex) 193 THz from ref 23; (Ex) 214 THz from ref 24; (Ex) 243 THz from ref 15; (Ex) 250 THz from ref 25.

frequency over a lower frequency. The slightly different ENZ frequencies (permittivity curves) are the source of the beat-like transmittance and absorbance patterns in Figure 2a, which features a narrowed waist in the C-band and decreased perturbations toward higher frequencies (see Supporting Information S1.5). The FSR of the sample is far higher than the FSR of the generated frequency combs, which will not affect the ML operation within a certain thickness range of the silica substrate (Supporting Information S2.3).

It is worth mentioning that although such linear selectivity conditions induced by our sample structure look similar to previous reports of intracavity ENZ experiments,[6,21,30] the underlying design principles and the resulting effects here are quite different. In the previous works, the fiber laser system could perform: (i) a short-range shift of ≈200 GHz by Q-switching;[30] (ii) a long-range shift of ≈2.21 THz by ML in a much more complex scheme;[21] or (iii) in a similar setup to this work, CW output without ENZ element, Q-switched output with an ENZ metasurface, and ≈1.46-THz-shifted Q-switched vortex-pulse output by adjusting focus.[6] It is challenging to include both long- and short-range frequency shifts in a single system while also obtaining a larger shift value. The key to this challenge is to utilize the ENZ-induced optical properties outside of the ENZ region. As mentioned, the ENZ frequencies of our sample are detuned from the laser operation. This frequency detuning helps bring a near-zero group-velocity dispersion (GVD) at the C-band[10,33] as compared to operating in a rapidly varying ultralarge GVD pattern near the ENZ frequencies at 2-μm-band (see Supporting Information S1.5). This feature makes the GVD more uniform in the C-band for both long- and short-range frequency shifts, and the FP structure of the sample allows more interaction time and volume, unlike the conditions in the previous reports. The GVD also decreases with frequency, which is consistent with the aforementioned ENZ-induced linear selectivity.

In the right panel of Figure 2a, an intermediate ML state exists for the long-range shift, which is presented in Figure 2b. During the ENZ-element switching, we record this metastable intermediate state with a slightly shifted ML state from the original position along with a new CW component at the destined frequency. This CW spectral component is different from the pre-ML one shown in Figure 1c, with the features of a four-wave-mixing (FWM) CW spectrum,[34−36] suggesting the effect of a third-order nonlinearity. However, given the level of intracavity intensity (0.53 GW·cm^{-2}) and a relatively large spot size (0.5 mm in diameter, full-width-at-half-maximum), the Kerr nonlinearity is expected to be too weak[37] to generate effective and observable FWM (see Supporting Information S1.4). A possible explanation could be the broadband ENZ enhancement of the thermo-optic nonlinearity[10] which covers the C-band and still needs to be investigated (see Supporting Information 1.5). For the short-range shift, we also recorded a similar FWM-like CW spectrum but without the coexistence of an intermediate ML component before the new ML state is established, as plotted in Figure 2c. We emphasize that the observed nonlinear phenomenon does not directly shift the frequency adiabatically like in the extracavity time-varying ENZ media,[15,23−25] but it rather participates in the rebuildup process of the soliton, as later discussed in Figure 4. When the pump power is increased, the pulse train splits into multiple solitons, clearly visible from recorded time traces, indicating completely different mechanisms between intracavity and extracavity ENZ-induced frequency shifts.

The major difference between the two initial laser states that results in the input-dependent dual-range frequency switching operations is where their central frequencies are located, much more than how they influence the ENZ nonlinear effects. From the perspective of intracavity ENZ nonlinear frequency shift, the difference between these two states is negligible: as shown in Table S2 in Supporting Information, the contributions of the two major factors, initial frequency and pulse fluence, are nearly equal. Instead, their central frequencies are located distinctly in the erbium gain spectrum (192 THz at the red end and 196 THz at the blue end, corresponding to the 191−196 THz gain region), resulting in significant differences in the margin reserved for frequency shift (mode reselection) within the resonant cavity environment.

Conversion Efficiencies. To assess and demonstrate the advantages of the intracavity design, namely, the requirements for pulse energy and material thickness, we define the following Figure-of-Merit (FoM) to compare the frequency conversion efficiency between intracavity and extracavity systems in terms of required pulse energy and ENZ material thickness.

https://doi.org/10.1021/acsphotonics.4c01322
ACS Photonics 2025, 12, 1276−1283

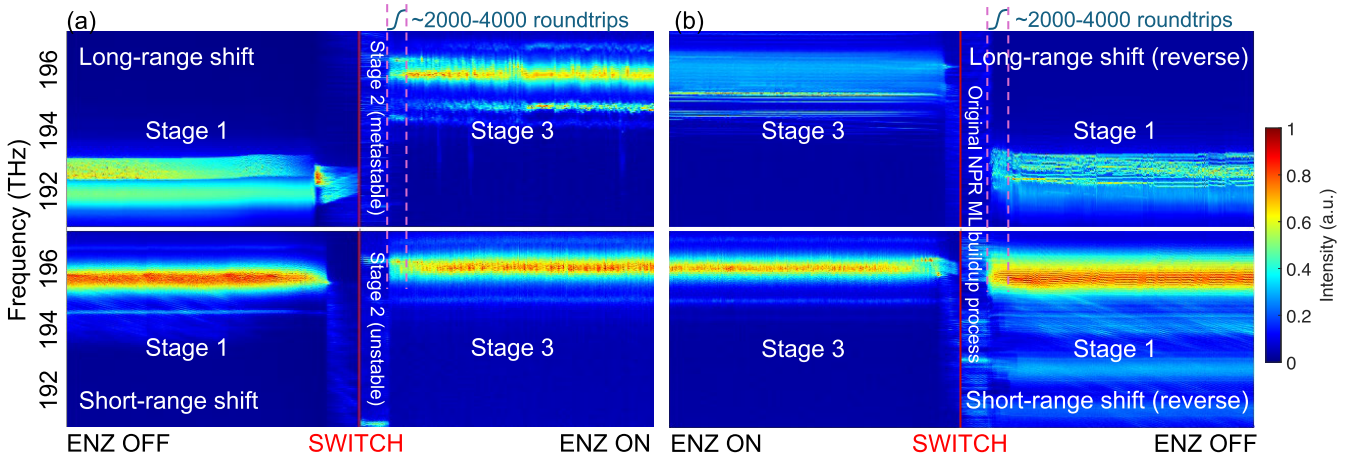

Figure 4. Real-time observation of the intracavity mode-lock (ML) frequency switch operation. Real-time evolution of (a) the long- and short-range ML frequency shifts; (b) the reverse processes.

$$\mathrm{FoM} = \frac{\Delta\nu}{\nu_0 E_{\mathrm{pulse}} d_{\mathrm{ENZ}}} \approx \frac{\Delta\nu}{\nu_0 I_{\mathrm{pulse}} \tau_{\mathrm{pulse}} d_{\mathrm{ENZ}}} \quad (1)$$

The dimension of the FoM is the conversion ratio per energy density per thickness of the material ($[\mathrm{J\cdot cm^{-2}}]^{-1}\ \mathrm{nm^{-1}}$). The first part of the FoM, $\Delta\nu/\nu_0$, is the dimensionless conversion ratio, noting the extent of frequency shift with respect to its original frequency. This is to achieve a relatively fair comparison across the different optical bands. E_{pulse} is the pulse fluence taken into account peak intensity density I_{pulse} usually measured in $\mathrm{GW\cdot cm^{-2}}$ and the full-width-at-half-maximum (fwhm) intensity temporal width τ_{pulse} of the pulse. d_{ENZ} is the thickness of the ENZ TCO materials used. This FoM definition is similar to the one used in ENZ extracavity adiabatic temporal-refraction-based frequency conversion[14] with the form $\Delta\nu/(\nu Id)$, but here the use of the pulse energy density instead of intensity density is more suitable to reflect the energy requirements across different platforms.

The calculated FoMs for various intracavity and extracavity reports are presented in Figure 3a (Supporting Information S2.1). Although inside a resonant active cavity, the intracavity pulse energy is still much lower in fiber lasers (ML: this work; Q-switched: ref 30) than in solid-state lasers. Attributed to the accumulative effect inside a cavity with abundant frequency resources, the ENZ material thickness is sufficient at the level of a hundred nanometers, hence the high FoM. By eq 1, the FoMs for the long- and short-range frequency shifts are 2 orders of magnitude higher than extracavity ENZ frequency shifts and 1 order of magnitude higher than intracavity ENZ Q-switching.[30]

The two aspects of the FoM can be decoupled into energy efficiency $\Delta\nu/(\nu_0 E_{\mathrm{pulse}})$ and thickness efficiency $\Delta\nu/(\nu_0 d_{\mathrm{ENZ}})$ to denote the frequency conversion percentage per unit energy density or thickness. The results are listed in Figure 3b. The short-range shift in this work and the reported Q-switched cavity have an energy efficiency on par with the extracavity studies, but their thickness efficiencies are lower. Note that the horizontal axis of Figure 3b is in linear scale, while the vertical axis is in logarithmic scale, which means that the difference in thickness efficiencies is within an order of magnitude. On the other hand, the long-range shift in this work is leading in both energy and thickness efficiencies, demonstrating the benefits of the intracavity design with the additional bonus of having dual-range frequency switching operations which has not been achieved before.

Real-Time Observation of Intracavity Frequency Switching. For the assessment of the intracavity ML buildup dynamics and mechanism, we employ the TS-DFT technique[38,39] for the first time in an ENZ laser cavity, to observe in real-time the frequency switch operations. TS-DFT can realize frame-by-frame discrete Fourier transform by simply relying on dispersion compensation, enabling the capture and recording of intracavity pulse evolution via a high-speed oscilloscope (see Supporting Information S3.2). In Figure 4 we show the experimental TS-DFT data of four processes, namely, switching the ENZ element OFF to ON for the long- and short-range ML frequency shifts and their reverse operations.

From Figure 4, the buildup of the ML states after switching is within 2000 to 4000 roundtrips, corresponding to <64 μs of operation time. The buildup time is estimated from the CW state, where it starts to grow until an ML pulse is stably formed. The total switching time consists of two parts: the ML state buildup time which is intrinsic to the cavity and the light path switching time (no ENZ to ENZ, and vice versa) which depends on the switching method used. In this proof-of-principle experiment, we used a mechanical switch, whose speed can be improved orders of magnitude faster by using an all-optical or electro-optical directional coupler in photonic integration.

Figure 4a indicates that a CW state is present between each switch action before the new ML state is formed, which is consistent with the intermediate CW states shown in Figure 2b,c. The duration marked with a red line in Figure 4 depends on the response time of the directional sample switch component before the ENZ, irrelevant to the ENZ element. As can be seen from Figure 4, the buildup processes of ML states with the intracavity ENZ element switched ON and OFF are, in general, similar but different in terms of the spectral-temporal patterns and dynamics due to the different real-time intracavity conditions.

The results in Figure 4 prove that the intracavity frequency switch operation is not adiabatic and different from the extracavity ENZ temporal refractions. The ENZ element does not steer the original ML frequency continuously to the new one but alters the intracavity mode-competition selectivity by its ENZ-induced linear and nonlinear optical characteristics

https://doi.org/10.1021/acsphotonics.4c01322
ACS Photonics 2025, 12, 1276−1283

shown in Figure 2a, which should be analyzed as a whole and cannot be decoupled.

Dual-Range-Frequency-Switching-Enabled Complex Logic Functions: A Potential Application Scheme. Photonic computing, logic gates,[40] and the emerging neuromorphic photonics[41,42] are important and timely topic of investigations, offering energy-efficient and elegant solutions with reduced system complexity compared to microelectronic devices, circuits, and chips. In this vein, the dual-range intracavity ML frequency switch operations can enable the frequency multiplexing needed for complex logic functions in photonic computing with only a few intracavity components.

Here, if we consider one of the binary states to be the 192 THz ML state and treat both the 196 THz ML states (initial and the 279.73-GHz shifted) as the other binary state, a frequency encoder/decoder can be defined. These two different 196 THz ML states are also a frequency multiplexing feature of the system allowing differentiation between the operated and the original unoperated outputs.

For the ENZ element as a permanent component of the cavity, if we encode 196 THz as 1 and 192 THz as 0, a one-operand TRUE gate is realized. Its reverse encoding results in a FALSE gate. For 2-operand (p, q) logic functions, the polarization control is one of the operands while the existent state of the intracavity ENZ component is another. Operating on the polarization control leads to setting an initial ML state of 192/196 THz, which can then be encoded (1,0) or (0,1) as one of the operation input p. Likewise, the existence/absence of the intracavity ENZ component can be encoded (1,0) or (0,1) as another operation input q. The laser output is the logic operation output, decoded by the same frequency encoding protocol as the initial ML state.

By permutation and combination, there are eight total possibilities, with two pairs of commutative OR and AND gates (i.e., p op q = q op p) and four noncommutative logic gates (i.e., p op $q \neq q$ op p), including *converse nonimplication* ($p \not\leftarrow q$), *material implication* (material conditional, $p \rightarrow q$), *material nonimplication* (abjunction, $p \not\rightarrow q$), and *converse implication* ($p \leftarrow q$). A full schematic and the truth table of all presented logic functions are available in Supporting Information S2.5. This implementation is programmable for multipurpose and different from the classical photonic logic gate designs.

DISCUSSION AND CONCLUSIONS

To improve the performance of the system, one could consider shortening the laser cavity, until the final goal of fully on-chip integration of the ML laser system.[43] The pump source[44] and the gain medium[32] can be integrated owing to the recent advancement in integrated optics, while several on-chip solutions for polarization controls have already been demonstrated.[45−47] The mechanical switch holding the ENZ element can be replaced in integrated circuits with an all-optical ENZ directional coupler design.[48] Such a system would result in FSRs up to tens of gigahertz instead of megahertz. It is worth noting that the ML frequency switch buildup time is measured in terms of the numbers of round-trips, which means a gigahertz system is expected to have orders of magnitude faster logic computation time. Still, system-wide integration is not an easy task to accomplish, and it is beyond the scope of this work. However, the advantages of such integration are not limited to the high FSR but also increased Kerr and thermo-optic nonlinearity due to a much smaller mode size, which can give rise to richer, more complex, and hybrid nonlinear phenomena.

In conclusion, in this work, we experimentally demonstrate for the first time the realization of efficient dual-range ML frequency switching by a single intracavity ENZ FP nanostructure with ML frequency multiplexing characteristics. Based on the initial cavity status, it can induce a long- or short-range ML frequency shift, which is not achievable in the cavity's continuously tunable range. Moreover, we employ the TS-DFT technique to investigate the real-time dynamics of the ENZ intracavity frequency switching operation for the first time, proving that the phenomena originate from intracavity mode-selectivity alteration instead of time refraction. Finally, we discussed the possibility of ML frequency encoding, enabling the optical system to perform eight different logic functions, including four complex noncommutative 2-operand logics. We believe that the results of this work deepen the understanding of ENZ photonics and extend the applications of ENZ photonics outside the extracavity scenarios. Considering its compatibility with cutting-edge photonic integration and nanophotonic platforms, the proposed photonic system can be useful in novel and programmable multipurpose photonic logic computing, ultrafast optical signal processing, and versatile optical communications.

ASSOCIATED CONTENT

Supporting Information

The Supporting Information is available free of charge at https://pubs.acs.org/doi/10.1021/acsphotonics.4c01322.

Sample information (ellipsometry data, Drude model and parameters, scanning electron microscopy, mechanisms on intracavity mode-selectivity); System design considerations (FoM comparisons, ENZ nanolayers with other frequencies, impact of substrate thickness, extracavity analyses, truth table of logic operations); Cavity characteristics (temporal profile and ML threshold, TS-DFT, stability analyses) (PDF)

AUTHOR INFORMATION

Corresponding Authors

Jiaye Wu − *École Polytechnique Fédérale de Lausanne (EPFL), Photonic Systems Laboratory (PHOSL), Lausanne CH-1015, Switzerland;* orcid.org/0000-0002-0650-1274; Email: jiaye.wu@epfl.ch

Camille-Sophie Brès − *École Polytechnique Fédérale de Lausanne (EPFL), Photonic Systems Laboratory (PHOSL), Lausanne CH-1015, Switzerland*; Email: camille.bres@epfl.ch

Authors

Gang Wang − *École Polytechnique Fédérale de Lausanne (EPFL), Photonic Systems Laboratory (PHOSL), Lausanne CH-1015, Switzerland*

Marco Clementi − *École Polytechnique Fédérale de Lausanne (EPFL), Photonic Systems Laboratory (PHOSL), Lausanne CH-1015, Switzerland;* orcid.org/0000-0003-4034-4337

Ji Zhou − *École Polytechnique Fédérale de Lausanne (EPFL), Photonic Systems Laboratory (PHOSL), Lausanne CH-1015, Switzerland*

Chenxingyu Huang − *Tsinghua Shenzhen International Graduate School, Tsinghua University, Shenzhen 518055, China;* orcid.org/0000-0003-0095-6523

https://doi.org/10.1021/acsphotonics.4c01322
ACS Photonics 2025, 12, 1276−1283

Xuanyi Liu − *Tsinghua Shenzhen International Graduate School, Tsinghua University, Shenzhen 518055, China*
H. Y. Fu − *Tsinghua Shenzhen International Graduate School, Tsinghua University, Shenzhen 518055, China*
Qian Li − *School of Electronic and Computer Engineering, Peking University, Shenzhen 518055, China;* orcid.org/0000-0002-2396-7041

Complete contact information is available at: https://pubs.acs.org/10.1021/acsphotonics.4c01322

Author Contributions

J.W. conceived the original idea of this work and conducted the main experiments. G.W. helped with the autocorrelation and TS-DFT data acquisition and analyses. M.C. helped with the initial preparations of the experiment and extensive manuscript revision. J.Z. provided the initial laser design scheme and participated in the building of the setup. C.H. performed the SEM characterizations. X.L. provided consultation and optimization suggestions in the building of the setup. Q.L., H.Y.F., and C.-S.B. provided the experimental resources. All authors took part in analyzing the data. J.W. wrote the manuscript with inputs from others. M.C. and C.-S.B. provided in-depth reviews and discussions in revising the manuscript. C.-S.B. supervised the project and experiments. All authors have proofread the manuscript.

Funding

This work is supported by the Swiss National Science Foundation (Grant No. 200021−188605) (C.-S.B.), the Basic and Applied Basic Research Foundation of Guangdong Province (Grant No. 2021A1515012176) (Q.L.), and Tsinghua Shenzhen International Graduate School-Shenzhen Pengrui Young Faculty Program of Shenzhen Pengrui Foundation (Grant No. SZPR2023008) (H.Y.F.).

Notes

The authors declare no competing financial interest.

REFERENCES

(1) Kinsey, N.; DeVault, C.; Boltasseva, A.; Shalaev, V. M. Near-zero-index materials for photonics. *Nature Reviews Materials* **2019**, *4*, 742−760.
(2) Reshef, O.; De Leon, I.; Alam, M. Z.; Boyd, R. W. Nonlinear optical effects in epsilon-near-zero media. *Nature Reviews Materials* **2019**, *4*, 535−551.
(3) Wu, J.; Xie, Z. T.; Sha, Y.; Fu, H. Y.; et al. Epsilon-near-zero photonics: infinite potentials. *Photonics Research* **2021**, *9*, 1616.
(4) Liberal, I.; Lobet, M.; Li, Y.; Engheta, N. Near-zero-index media as electromagnetic ideal fluids. *Proc. Natl. Acad. Sci. U. S. A.* **2020**, *117*, 24050−24054.
(5) Li, H.; Zhou, Z.; Sun, W.; Lobet, M.; Engheta, N.; Liberal, I.; Li, Y. Direct observation of ideal electromagnetic fluids. *Nat. Commun.* **2022**, *13*, 4747.
(6) Jia, W.; Gao, C.; Zhao, Y.; Li, L.; Wen, S.; Wang, S.; Bao, C.; Jiang, C.; Yang, C.; Yang, Y. Intracavity spatiotemporal metasurfaces. *Advanced Photonics* **2023**, *5*, 026002.
(7) Xie, Z. T.; Sha, Y.; Wu, J.; Fu, H. Y.; et al. Ultrafast dynamic switching of optical response based on nonlinear hyperbolic metamaterial platform. *Opt. Express* **2022**, *30*, 21634−21648.
(8) Alam, M. Z.; De Leon, I.; Boyd, R. W. Large optical nonlinearity of indium tin oxide in its epsilon-near-zero region. *Science* **2016**, *352*, 795−797.
(9) Yang, Y.; Lu, J.; Manjavacas, A.; Luk, T. S.; et al. High-harmonic generation from an epsilon-near-zero material. *Nat. Phys.* **2019**, *15*, 1022−1026.
(10) Wu, J.; Clementi, M.; Huang, C.; Ye, F.; Fu, H.; Lu, L.; Zhang, S.; Li, Q.; Brès, C.-S. Thermo-optic epsilon-near-zero effects. *Nat. Commun.* **2024**, *15*, 794.
(11) Silveirinha, M.; Engheta, N. Tunneling of electromagnetic energy through subwavelength channels and bends using ε-near-zero materials. *Phys. Rev. Lett.* **2006**, *97*, 157403.
(12) Capretti, A.; Wang, Y.; Engheta, N.; Dal Negro, L. Enhanced third-harmonic generation in Si-compatible epsilon-near-zero indium tin oxide nanolayers. *Opt. Lett.* **2015**, *40*, 1500.
(13) Luk, T. S.; de Ceglia, D.; Liu, S.; Keeler, G. A.; et al. Enhanced third harmonic generation from the epsilon-near-zero modes of ultrathin films. *Appl. Phys. Lett.* **2015**, *106*, 151103.
(14) Khurgin, J. B.; Clerici, M.; Bruno, V.; Caspani, L.; et al. Adiabatic frequency shifting in epsilon-near-zero materials: the role of group velocity. *Optica* **2020**, *7*, 226.
(15) Zhou, Y.; Alam, M. Z.; Karimi, M.; Upham, J.; et al. Broadband frequency translation through time refraction in an epsilon-near-zero material. *Nat. Commun.* **2020**, *11*, 2180.
(16) Tian, W.; Liang, F.; Lu, D.; Yu, H.; et al. Highly efficient ultraviolet high-harmonic generation from epsilon-near-zero indium tin oxide films. *Photonics Research* **2021**, *9*, 317−323.
(17) Jia, W.; Liu, M.; Lu, Y.; Feng, X.; et al. Broadband terahertz wave generation from an epsilon-near-zero material. *Light Sci. Appl.* **2021**, *10*, 11.
(18) Minerbi, E.; Sideris, S.; Khurgin, J. B.; Ellenbogen, T. The Role of Epsilon Near Zero and Hot Electrons in Enhanced Dynamic THz Emission from Nonlinear Metasurfaces. *Nano Lett.* **2022**, *22*, 6194−6199.
(19) Campione, S.; de Ceglia, D.; Vincenti, M. A.; Scalora, M.; et al. Electric field enhancement in ε-near-zero slabs under TM-polarized oblique incidence. *Phys. Rev. B* **2013**, *87*, 035120.
(20) Wu, J.; Malomed, B. A.; Fu, H. Y.; Li, Q. Self-interaction of ultrashort pulses in an epsilon-near-zero nonlinear material at the telecom wavelength. *Opt. Express* **2019**, *27*, 37298−37306.
(21) Wu, J.; Liu, X.; Malomed, B. A.; Chang, K.-C.; et al. Observation of SQUID-Like Behavior in Fiber Laser with Intra-Cavity Epsilon-Near-Zero Effect. *Laser Photonics Reviews* **2022**, *16*, 2200487.
(22) Tirole, R.; Vezzoli, S.; Galiffi, E.; Robertson, I.; et al. Double-slit time diffraction at optical frequencies. *Nat. Phys.* **2023**, *19*, 999−1002.
(23) Liu, C.; Alam, M. Z.; Pang, K.; Manukyan, K.; Hendrickson, J. R.; Smith, E. M.; Zhou, Y.; Reshef, O.; Song, H.; Zhang, R.; Song, H.; Alishahi, F.; Fallahpour, A.; Almaiman, A.; Boyd, R. W.; Tur, M.; Willner, A. E. Tunable Doppler shift using a time-varying epsilon-near-zero thin film near 1550 nm. *Opt. Lett.* **2021**, *46*, 3444.
(24) Bruno, V.; Vezzoli, S.; DeVault, C.; Carnemolla, E.; Ferrera, M.; Boltasseva, A.; Shalaev, V. M.; Faccio, D.; Clerici, M. Broad Frequency Shift of Parametric Processes in Epsilon-Near-Zero Time-Varying Media. *Applied Sciences* **2020**, *10*, 1318.
(25) Bohn, J.; Luk, T. S.; Horsley, S.; Hendry, E. Spatiotemporal refraction of light in an epsilon-near-zero indium tin oxide layer: frequency shifting effects arising from interfaces. *Optica* **2021**, *8*, 1532.
(26) Wood, M. G.; Campione, S.; Parameswaran, S.; Luk, T. S.; et al. Gigahertz speed operation of epsilon-near-zero silicon photonic modulators. *Optica* **2018**, *5*, 233.
(27) Rajput, S.; Kaushik, V.; Babu, P.; Pandey, S. K.; Kumar, M. All optical modulation in vertically coupled indium tin oxide ring resonator employing epsilon near zero state. *Sci. Rep.* **2023**, *13*, 18379.
(28) Jiang, X.; Lu, H.; Li, Q.; Zhou, H.; et al. Epsilon-near-zero medium for optical switches in a monolithic waveguide chip at 1.9 μm. *Nanophotonics* **2018**, *7*, 1835−1843.
(29) Xiao, Q.-H.; Feng, X.-Y.; Yang, W.; Lin, Y.-K.; et al. Epsilon-near-zero indium tin oxide nanocolumns array as a saturable absorber for a Nd:BGO laser. *Laser Physics* **2020**, *30*, 055802.
(30) Zhang, C.; Zu, Y.; Yang, W.; Jiang, S.; et al. Epsilon-near-zero medium for optical switches in Ho solid-state laser at 2.06 μm. *Optics & Laser Technology* **2020**, *129*, 106271.
(31) Guo, Q.; Cui, Y.; Yao, Y.; Ye, Y.; et al. A solution-processed ultrafast optical switch based on a nanostructured epsilon-near-zero medium. *Adv. Mater.* **2017**, *29*, 1700754.

(32) Liu, Y.; Qiu, Z.; Ji, X.; Lukashchuk, A.; He, J.; Riemensberger, J.; Hafermann, M.; Wang, R. N.; Liu, J.; Ronning, C.; Kippenberg, T. J. A photonic integrated circuit−based erbium-doped amplifier. *Science* **2022**, *376*, 1309−1313.
(33) Wu, J.; Xie, Z. T.; Sha, Y.; Fu, H. Y.; et al. Comparative study on epsilon-near-zero transparent conducting oxides: High-order chromatic dispersions and modeling of ultrashort pulse interactions. *Phys. Rev. A* **2020**, *102*, 053503.
(34) Luo, Z.; Zhou, M.; Wu, D.; Ye, C.; Weng, J.; Dong, J.; Xu, H.; Cai, Z.; Chen, L. Graphene-Induced Nonlinear Four-Wave-Mixing and Its Application to Multiwavelength Q-Switched Rare-Earth-Doped Fiber Lasers. *Journal of Lightwave Technology* **2011**, *29*, 2732−2739.
(35) Debnath, P. C.; Uddin, S.; Song, Y.-W. Ultrafast All-Optical Switching Incorporating in Situ Graphene Grown along an Optical Fiber by the Evanescent Field of a Laser. *ACS Photonics* **2018**, *5*, 445−455.
(36) Zhao, Q.; Pei, L.; Tang, M.; Xie, Y.; Ruan, Z.; Zheng, J.; Ning, T. Switchable multi-wavelength erbium-doped fiber laser based on core-offset structure and four-wave-mixing effect. *Optical Fiber Technology* **2020**, *54*, 102111.
(37) Huang, C.; Peng, S.; Liu, X.; Wu, J.; et al. Manufacturing-Enabled Tunability of Linear and Nonlinear Epsilon-Near-Zero Properties in Indium Tin Oxide Nanofilms. *ACS Appl. Mater. Interfaces* **2023**, *15*, 35186−35195.
(38) Goda, K.; Jalali, B. Dispersive Fourier transformation for fast continuous single-shot measurements. *Nat. Photonics* **2013**, *7*, 102−112.
(39) Mahjoubfar, A.; Churkin, D. V.; Barland, S.; Broderick, N.; Turitsyn, S. K.; Jalali, B. Time stretch and its applications. *Nat. Photonics* **2017**, *11*, 341−351.
(40) McMahon, P. L. The physics of optical computing. *Nature Reviews Physics* **2023**, *5*, 717−734.
(41) Shastri, B. J.; Tait, A. N.; Ferreira de Lima, T.; Pernice, W. H. P.; Bhaskaran, H.; Wright, C. D.; Prucnal, P. R. Photonics for artificial intelligence and neuromorphic computing. *Nat. Photonics* **2021**, *15*, 102−114.
(42) Feldmann, J.; Youngblood, N.; Karpov, M.; Gehring, H.; Li, X.; Stappers, M.; Le Gallo, M.; Fu, X.; Lukashchuk, A.; Raja, A. S.; Liu, J.; Wright, C. D.; Sebastian, A.; Kippenberg, T. J.; Pernice, W. H. P.; Bhaskaran, H. Parallel convolutional processing using an integrated photonic tensor core. *Nature* **2021**, *589*, 52−58.
(43) Gordón, C.; Guzmán, R.; Leijtens, X.; Carpintero, G. On-chip mode-locked laser diode structure using multimode interference reflectors. *Photonics Research* **2015**, *3*, 15.
(44) Clementi, M.; Nitiss, E.; Liu, J.; Durán-Valdeiglesias, E.; Belahsene, S.; Debrégeas, H.; Kippenberg, T. J.; Brès, C.-S. A chip-scale second-harmonic source via self-injection-locked all-optical poling. *Light Sci. Appl.* **2023**, *12*, 296.
(45) Velha, P.; Sorianello, V.; Preite, M. V.; De Angelis, G.; Cassese, T.; Bianchi, A.; Testa, F.; Romagnoli, M. Wide-band polarization controller for Si photonic integrated circuits. *Opt. Lett.* **2016**, *41*, 5656.
(46) Hou, Z.; Xiong, X.; Cao, J.; Chen, Q.; Tian, Z.; Ren, X.; Sun, H. On-Chip Polarization Rotators. *Advanced Optical Materials* **2019**, *7*, 7.
(47) Zhao, W.; Peng, Y.; Zhu, M.; Liu, R.; Hu, X.; Shi, Y.; Dai, D. Ultracompact silicon on-chip polarization controller. *Photonics Research* **2024**, *12*, 183.
(48) Sha, Y.; Xie, Z. T.; Wu, J.; Fu, H. Y.; et al. All-optical switching in epsilon-near-zero asymmetric directional coupler. *Sci. Rep.* **2022**, *12*, 17958.

https://doi.org/10.1021/acsphotonics.4c01322
ACS Photonics 2025, 12, 1276−1283